Nuclear Science and Techniques (2024) 35:165
https://doi.org/10.1007/s41365-024-01555-6

Analysis of level structure and monopole effects in Ca isotopes

Jin Li[1] · Ai-Xi Chen[1] · Amir Jalili[1] · Han-Kui Wang[1]

Received: 21 March 2024 / Revised: 17 June 2024 / Accepted: 2 July 2024 / Published online: 18 September 2024

Abstract

Understanding the properties of nuclei near the double magic nucleus ^{40}Ca is crucial for both nuclear theory and experiments. In this study, Ca isotopes were investigated using an extended pairing-plus-quadrupole model with monopole corrections. The negative-parity states of ^{44}Ca were coupled with the intruder orbital $g_{9/2}$ at 4 MeV. The values of E_{4+}/E_{2+} agree well with experimental trend from ^{42}Ca to ^{50}Ca, considering monopole effects between $\nu f_{7/2}$ and $\nu p_{3/2}(\nu f_{5/2})$. This monopole effect, determined from data of ^{48}Ca and ^{50}Ca, supports the proposed new nuclear magic number $N = 34$ by predicting a high-energy 2^+ state in ^{54}Ca.

Keywords Shell model · Doubly magic · Isotopes · Monopole effects · Level structure

1 Introduction

Nuclei northeast of double magic nucleus ^{40}Ca are of significant interest in both experiments and shell model theory. The research in Ref. [1] highlighted the doubly magic nature of ^{54}Ca and provided direct experimental evidence for the onset of a sizable subshell closure at $N = 34$. Possible variations of magic numbers have attracted considerable interest in nuclear physics [2, 3]. For exotic nuclei, the universality of magic numbers does not extend to stable nuclei; some nuclei lose their magic properties [4–8], whereas others acquire new magic numbers [1, 8–12]. The significantly larger cross-section observed in ^{53}Ca provides direct evidence for the $N = 34$ shell closure. [13]. Interaction cross sections for $^{42–51}$Ca were measured for the first time on a carbon target at 280MeV per nucleon [14]. A recent publication [15] showcased cutting-edge experimental and theoretical advancements related to 2p decay, including technological innovations for measuring nucleon-nucleon correlations and developments in models linking structural attributes and decay properties.

Charge resolution is crucial for particle identification in ionization measurement system (IMS) experiments involving ion pairs [16]. Additionally, Ref. [17] predicted the cross sections of ejectile residues (ERIs) in 140MeV/u projectile fragmentation reactions with ^{78,86}Kr / ^{58,64}Ni / ^{40,48}Ca + ^{9}Be using the proposed model. Another study [18] applied the continuum Skyrme Hartree–Fock–Bogoliubov (HFB) theory with Green's function method to study neutron-rich Ca, Ni, Zr, and Sn isotopes, accurately reproducing the experimental double- and single-neutron separation energies. Lastly, Ref. [19] utilized a dinuclear system model to explore reactions of ^{40,48}Ca projectiles with ^{238}U, ^{242}Pu, and ^{243}Am targets at various incident energies. This study analyzed the dependence of calculated synthesis cross sections on collision orientations, discussed the isospin effect of projectiles, and explored the influence of entrance channel effects on the synthesis cross sections of superheavy nuclei.

In theoretical studies, determining the half-lives of β decay and β delayed neutron emission (βn) is crucial for advancing fundamental science, nuclear physics, and industrial applications [20]. By including contributions of the three-body force, the effective shell model Hamiltonian can reproduce the experimental shell evolution toward and beyond the closure at $N = 28$ [21].

Examinations of the excited states in Ti isotopes have been performed within a single j-shell framework [22].

This work was supported by the National Natural Science Foundation of China (Nos.12175199, U2267205, 12475124) and the ZSTU intramural grant (22062267-Y).

✉ Ai-Xi Chen
aixichen@zstu.edu.cn

✉ Han-Kui Wang
whk2007@163.com

1 School of Science, Zhejiang Sci-Tech University, Hangzhou 310018, China

Comparative research on *pf* shell nuclei has been conducted using both the cranked Nilsson–Strutinsky model and the spherical shell model [23]. Over the past few decades, various models have been designed to analyze the spectroscopic properties of atomic nuclei. Large-scale spherical shell model calculations, such as those for a set of interactions [24], show excellent agreement with observed data. Based on existing interactions, this Hamiltonian utilizes the *pf* shell as the valence shell. More recently, the EPQQM model, initially designed for $N \approx Z$ nuclei by Hassegawa and Kaneko [25], has proven effective in different mass regions, including proton-rich *pf* shells [26], $pf_{5/2}g_{9/2}$ shells [27], neutron-rich *fpg* shells [28], and $sd - pf$ shells [29]. In the heavy neutron enrichment region near $A = 130$, the EPQQM model successfully elucidated low-energy and high-core excitations [30–32], confirming the persistence of the $N = 82$ shell closure. In addition, it provides a comprehensive description of the ground-state inversions driven by monopole interactions between protons and neutrons [33–35].

In nuclear physics, the intruder orbit $g_{9/2}$ plays a significant role in connecting the *df* and *pf* shells. Intruder states, which extend beyond valence configurations, significantly affect the structural properties of atomic nuclei. They can cause inversions in ground-state or low-lying excited-state, altering the energy level order predicted by the conventional shell model. Intruder states also influence various nuclear properties, including energy and structure. The Ref. [36] studied nuclei near a double magic nucleus ^{40}Ca using the intruder orbit $g_{9/2}$ and successfully reproduced the low level positive-parity states of ^{42}Ca, ^{42}Sc, and $^{42–44}$Ti, while predicting the negative-parity level. This confirms that the intruder orbit $g_{9/2}$ is crucial for studying high-energy state near the double magic nucleus ^{40}Ca. Furthermore, the intruder orbit $i_{13/2}$ plays a crucial role [37] in the Sn isotope chain. In this study, the EPQQM model, including the intruder orbit $g_{9/2}$, was used to explore the nuclear energy levels in ^{44}Ca. The inclusion of the intruder orbit provides a comprehensive description of the positive-parity and high-energy states with negative parity in these nuclei.

The model's calculations were compared with experimental results to validate its accuracy, emphasizing the importance of including intruder states in nuclear structure. Intruder states may be linked to shape coexistence, where different shapes coexist in the ground state of a nucleus due to the mixing of distinct configurations [38, 39]. This phenomenon is observed in numerous atomic nuclei, and integrating intruder states into the model space offers a more comprehensive depiction of shape coexistence. Such considerations are crucial for comprehending the evolution of nuclear shape in response to variations in neutron or proton numbers and for investigating the potential presence of novel magic numbers.

Notably, in the EPQQM model, particularly for unstable nuclei near ^{132}Sn, the inclusion of a monopole correction led to the development of a new Hamiltonian above ^{132}Sn, incorporating both core excitation and the intruder orbit $i_{13/2}$. This enhanced model successfully elucidates low-lying and high-spin excitations, and predicts and confirms the anti-aligned low-lying excitations in ^{129}Cd. By encompassing the cross-shell orbitals, the model overcomes limitations associated with closed-shell interactions, rendering it suitable for investigating high-spin spectra in unstable nuclei. Furthermore, careful selection of the model space, considering single-particle energies, is paramount for ensuring the accuracy of the shell model calculations.

This study utilized the EPQQM model, incorporating the $g_{9/2}$ intruder orbit within the *pf* shell model space to investigate the level spectra of ^{44}Ca. The EPQQM interaction effectively describes the positive-parity levels and intruder states in these isotopes, offering configurations for negative-parity levels. The calculations were performed using the NUSHELLX@MSU shell model code [40].

2 Hamiltonian

In the proton-neutron (*pn*) representation, the EPQQM Hamiltonian consists of pairing forces, multipole terms, and monopole corrections [26, 32, 36]:

$$
\begin{aligned}
H =& H_{\mathrm{sp}} + H_{P_0} + H_{P_2} + H_{QQ} + H_{OO} + H_{HH} + H_{\mathrm{mc}} \\
=& \sum_{\alpha,i} \varepsilon_a^i c_{\alpha,i}^\dagger c_{\alpha,i} - \frac{1}{2} \sum_{J=0,2} \sum_{ii'} g_{J,ii'} \sum_M P_{JM,ii'}^\dagger P_{JM,ii'} \\
& -\frac{1}{2} \sum_{ii'} \frac{\chi_{2,ii'}}{b^4} \sum_M : Q_{2M,ii'}^\dagger Q_{2M,ii'} : \\
& -\frac{1}{2} \sum_{ii'} \frac{\chi_{3,ii'}}{b^6} \sum_M : O_{3M,ii'}^\dagger O_{3M,ii'} : \\
& -\frac{1}{2} \sum_{ii'} \frac{\chi_{4,ii'}}{b^8} \sum_M : H_{4M,ii'}^\dagger H_{4M,ii'} : \\
& + \sum_{a \le c,ii'} k_{\mathrm{mc}}(ia, i'c) \sum_{JM} A_{JM}^\dagger(ia, i'c) A_{JM}(ia, i'c).
\end{aligned} \tag{1}
$$

The effective interaction (1) encompasses the single-particle Hamiltonian (H_{sp}), $J = 0$ and $J = 2$ pairing terms ($P_0^\dagger P_0$ and $P_2^\dagger P_2$), quadrupole-quadrupole interactions ($Q^\dagger Q$), octupole-octupole interactions ($O^\dagger O$), hexadecapole-hexadecapole interactions ($H^\dagger H$), and monopole corrections (H_{mc}). In the *pn* representation, $P_{JM,ii'}^\dagger$ and $A_{JM}^\dagger(ia, i'c)$ serve as pair operators, while $Q_{2M,ii'}^\dagger$, $O_{3M,ii'}^\dagger$, and $H_{4M,ii'}^\dagger$ represent the quadrupole, octupole, and hexadecapole operators. Here, i (i') denotes the nucleon index, where i is a proton, and i' is a neutron. The parameters $g_{J,ii'}$, $\chi_{2,ii'}$, $\chi_{3,ii'}$, $\chi_{4,ii'}$, and $k_{\mathrm{mc}}(ia, i'c)$ represent the respective strengths of forces, and b

Table 1 Two-body force strengths (in MeV) used in the present calculation. [36]

ii'	$g_{0,ii'}$	$g_{2,ii'}$	$\chi_{2,ii'}$	$\chi_{3,ii'}$	$\chi_{4,ii'}$
pp	0.450	0.470	−0.107	0.075	0.0010
nn	0.422	0.449	0	0.075	0.0010
pn	0	0	0.256	0	0.0009

is the range parameter of the harmonic oscillator. The model space for protons (neutrons) includes the entire *pf* shell orbitals ($1f_{7/2}, 1f_{5/2}, 2p_{1/2}, 2p_{3/2}$) with a core nucleus of ^{40}Ca. In addition, the $1g_{9/2}$ orbital is introduced as an intruder state to study high-energy levels.

The two-body force strengths of the EPQQM model are presented in Table 1 [36]. The parameters of the proton (neutron) $J = 0$ and $J = 2$ pairing forces were confirmed using data from 2^+, 4^+, and 6^+ in ^{42}Ti (^{42}Ca). Quadrupole-quadrupole and octupole-octupole forces significantly affect spectra with more than two valence particles, such as $^{42-44}$Ti. The hexadecapole-hexadecapole force primarily affected the high-spin levels. The parameters between protons and neutrons were confirmed by the odd-odd nuclear ^{42}Sc. In Ref. [36], two monopole correction terms were added to modify the monopole force between orbits $1f_{7/2}$ and $1g_{9/2}$ as $Mc1 \equiv k_{\rm mc}(\nu f_{7/2}, \nu g_{9/2}) = -1.10$ MeV, and $Mc2 \equiv k_{\rm mc}(\pi f_{7/2}, \pi g_{9/2}) = -1.10$ MeV. In this study, we increased the monopole term $Mc3(Mc4)$ to modify the energy gap between the neutron orbits $2p_{3/2}(1f_{5/2})$ and $1f_{7/2}$.

$$\begin{aligned} Mc3 &\equiv k_{\rm mc}(\nu f_{7/2}, \nu p_{3/2}) = 0.18\,\text{MeV}, \\ Mc4 &\equiv k_{\rm mc}(\pi f_{7/2}, \pi f_{5/2}) = 0.65\,\text{MeV}. \end{aligned} \tag{2}$$

The strengths are determined by the 2^+ states in ^{48}Ca and ^{50}Ca and their monopole effects are discussed in Sect. 3.2.

3 Results and discussion

3.1 Level spectra of $^{44-58}$Ca

In this section, we investigate the level spectra of $^{44-58}$Ca, including the $g_{9/2}$ orbitals in ^{44}Ca and ^{46}Ca. As shown in Fig. 1a, shell model calculations revealed the shared major configurations of ^{44}Ca in the ground and excited states (2^+, 4^+, and 6^+). However, differences emerged in minor configurations, notably in the ground-state composition. For the second 2^+ state, the EPQQM and a set of interactions exhibited varying configurations. The EPQQM model predicted the second 4^+ states with 79.44% $\nu f^4_{7/2}$ and 4.97% $\nu f^3_{7/2}p_{3/2}$, whereas the set of effective interactions had a higher predominance of approximately 96.15% $\nu f^4_{7/2}$. For negative-parity states, the EPQQM model accurately predicts 3^-, 4^-,

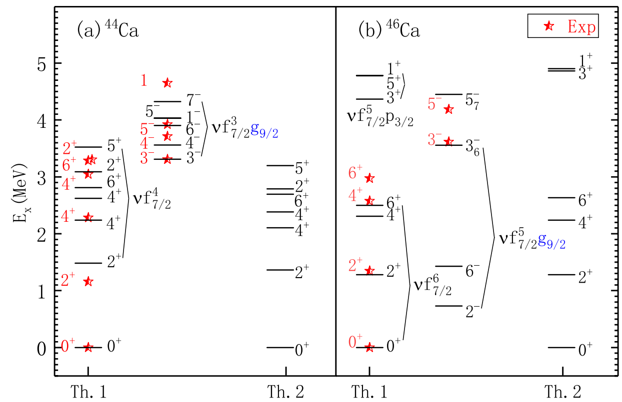

Fig. 1 Experimental states of ^{44}Ca and ^{46}Ca [41], and the shell model calculations by EPQQM (Th.1) and a set of effective interactions (Th.2)

and 5^- states with the $\nu f^3_{7/2}g_{9/2}$ configuration. The set of effective interactions failed to reproduce negative-parity states due to the absence of cross-shell and intruder orbits in the model space.

Recent studies on Ca isotopes have explored the nuclear entropy, revealing an approximate particle-hole symmetry between ^{42}Ca and ^{46}Ca. In the current model space, calculations for states (0^+, 2^+, 4^+, and 6^+) show shape-coexistence configurations. For the 4^+ level coupled with the $\nu f^6_{7/2}$ configuration, the calculated energy closely aligns with the experimental value of 2.574 MeV. Figure 1b shows a primary $\nu f^6_{7/2}$ configuration for the ground state and excited states (2^+, 4^+, 6^+), and another shared configuration for the excited states (1^+, 3^+, 5^+). Calculated using EPQQM and a set of effective interactions, some differences exist in the minor configurations. In the EPQQM model, the ground state 0^+ comprises roughly 79.21% of $\nu f^6_{7/2}$, 8.78% of $\nu f^4_{7/2}p^2_{3/2}$, and 4.34% of $\nu f^4_{7/2}f^2_{5/2}$. Conversely, the ground state 0^+ of a set of effective interactions was dominated by approximately 92.79% of $\nu f^6_{7/2}$.

In ^{48}Ca, stable properties are exhibited, featuring an excitation spectrum of up to 13 MeV. Ground-and excited-state calculations revealed coexistence features for the 2^+, 3^+, 4^+, and 5^+ states. As shown in Fig. 2a, the dominant configuration for the excited states is $\nu f^7_{7/2}p_{3/2}$, whereas the secondary configurations exhibit slight differences. The 1^+ state in the EPQQM model exhibits a primary configuration of $\nu f^6_{7/2}p^2_{3/2}$, with secondary configurations comprising 7.36% of $\nu f^6_{7/2}p_{3/2}p_{1/2}$ and 1.95% of $\nu f^7_{7/2}f_{5/2}$. Understanding these energy levels and configuration distributions is crucial for advancing our knowledge of nuclear structures.

In ^{50}Ca, the ground state has a short half-life of 13.45 s. As illustrated in Fig. 2b the excited states can reach 11 MeV

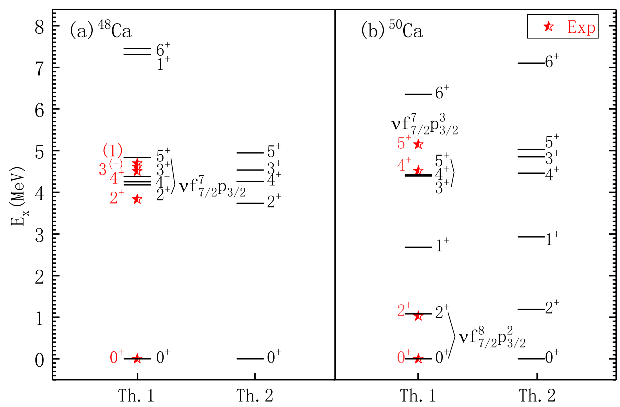

Fig. 2 Experimental states of ^{48}Ca and ^{50}Ca [41], and the shell model calculations by EPQQM (Th.1) and a set of effective interactions (Th.2)

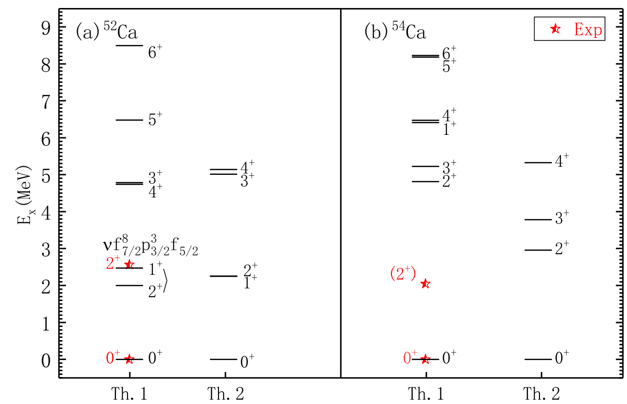

Fig. 3 Experimental states of ^{52}Ca and ^{54}Ca [41], and the shell model calculations by EPQQM (Th.1) and a set of effective interactions (Th.2)

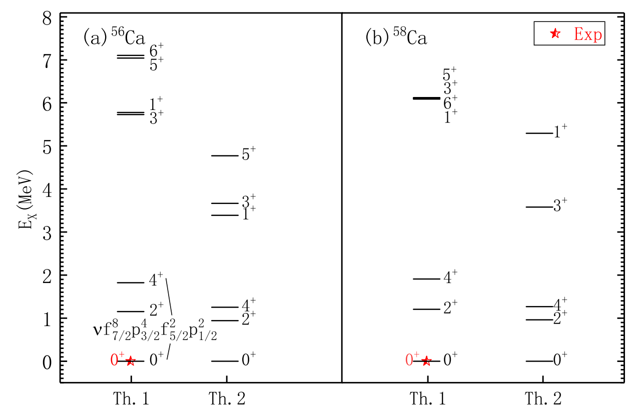

Fig. 4 Experimental states of ^{56}Ca and ^{58}Ca [41], and the shell model calculations by EPQQM (Th.1) and a set of effective interactions (Th.2)

with a maximum spin of 8^+. The coexistence configurations are shown in the ground state and the 2^+ excited state as $\nu f^8_{7/2}p^2_{3/2}$. Similarly, excited states 3^+, 4^+, and 5^+ have the same preliminary configuration. Figure 2b illustrates that the ground state 0^+ is primarily composed of approximately 74.61% of $\nu f^8_{7/2}p^2_{3/2}$ and 6.6% of $\nu f^6_{7/2}p^4_{3/2}$. The configuration of ground state 0^+ is dominated by approximately 86.92% of $\nu f^8_{7/2}p^2_{3/2}$ and 6.11% of $\nu f^8_{7/2}p^2_{1/2}$ in a set of effective interactions. The 2^+ excited state is primarily composed of 79.45% of $\nu f^8_{7/2}p^2_{3/2}$ whereas in a set of effective interactions, it predominantly consists of 85.72% of $\nu f^8_{7/2}p^2_{3/2}$. Notable differences in the secondary configurations were observed for the 4^+ and 5^+ energy levels. These findings enhance the understanding of the energy levels and configuration distributions of ^{50}Ca. Recent discoveries of neutron shell closures at $N = 32$ and $N = 34$ in the *pf*-shell region have been attributed to the filling of neutron orbits $2p_{1/2}$ and $2p_{3/2}$, respectively. These shell closures were determined based on observations related to the first 2^+ excitation energies, transition probabilities, mass measurements, $E(2^+)$, and neutron stripping cross sections.

For ^{52}Ca (Fig. 3a), the calculated results revealed shared primary features in the configurations of the 1^+ and 2^+ excited states. The EPQQM model exhibited increased secondary configurations for the ground state 0^+ and the 2^+ excited states. Specifically, the ground state 0^+ is predominantly composed of approximately 78.06% of $\nu f^8_{7/2}p^4_{3/2}$ and 8.12% of $\nu f^8_{7/2}p^2_{3/2}p^2_{1/2}$, whereas in a set of effective interactions, it primarily consists of approximately 83.11% $\nu f^8_{7/2}p^4_{3/2}$ and 11% of $\nu f^8_{7/2}p^2_{3/2}p^2_{1/2}$. For the 2^+ excited state, the EPQQM model is primarily composed of 84.83% of $\nu f^8_{7/2}p^3_{3/2}p_{1/2}$ and 4.94% of $\nu f^8_{7/2}p^2_{3/2}p^2_{1/2}$, while a set of effective interactions model predominantly consists of 89.51% of $\nu f^8_{7/2}p^3_{3/2}p_{1/2}$ and 4.12% of $\nu f^8_{7/2}p^2_{3/2}p^2_{1/2}$. Overall, the excited states 1^+, 2^+, 3^+, and 4^+ provide reliable predictions of the energy-level structure of ^{52}Ca within the model space calculations.

In Fig. 3b, the ground state 0^+ of ^{54}Ca is 91.64% $\nu f^8_{7/2}p^4_{3/2}p^2_{1/2}$, whereas in a set of effective interactions, it is 95.09%. The 2^+ state is 89.96% $\nu f^8_{7/2}p^4_{3/2}f_{5/2}p_{1/2}$, while in a set of effective interactions, the 2^+ state is 94.54% $\nu f^8_{7/2}p^4_{3/2}f_{5/2}p_{1/2}$. Predictions for the 3^+ and 4^+ states are provided, and the absence of negative-parity levels is due to the exclusion of the $g_{9/2}$ orbital when the model space dimension overflows.

For ^{56}Ca (Fig. 4a), the ground state and the 2^+ and 4^+ excited states have coexisting configurations. The 1^+ and 5^+ excited states exhibit consistent primary configurations across both the EPQQM and a set of effective interactions. Notable differences arise in the secondary configurations of the ground state and the 2^+ state between EPQQM and a set of effective interactions. At the 3^+ level, there is a variation in the primary configuration between the two interactions. Overall, these calculations provide insight into the predicted energy levels and configurations of ^{56}Ca.

Figure 4b shows the calculated results for the energy-level structure of ^{58}Ca. Due to the absence of experimental values for comparison, these results serve as predictions. In the EPQQM model, the ground state 0^+ is mainly composed of $\nu f^8_{7/2}p^4_{3/2}f^4_{5/2}p^2_{1/2}$ and $\nu f^6_{7/2}p^4_{3/2}f^6_{5/2}p^2_{1/2}$, while in a set of effective interactions, it is primarily $\nu f^8_{7/2}p^4_{3/2}f^4_{5/2}p^2_{1/2}$. For the 2^+ state, both models show the dominance of $\nu f^8_{7/2}p^4_{3/2}f^4_{5/2}p^2_{1/2}$. The 4^+ and 3^+ states are primarily $\nu f^8_{7/2}p^4_{3/2}f^4_{5/2}p^2_{1/2}$ and $\nu f^7_{7/2}p^4_{3/2}f^5_{5/2}p^2_{1/2}$. The EPQQM with the monopole effects of $Mc3$ and $Mc4$ accurately reproduces the level structure of Ca isotopes from $N = 22$ to $N = 30$ and predicts some useful states in $^{52-58}$Ca in the absence of experimental data.

3.2 The level spectra and $B(E2)$ with monopole effects

In this section, the analysis of E_{2+} and E_{4+} span isotopes from ^{42}Ca to ^{58}Ca (Fig. 5). As indicated by the gray points in ^{42}Ca, the interaction in Ref. [36] plays an important role in nuclei close to ^{40}Ca. After the neutron number increased, the 2^+ levels increased to approximately 3.8 MeV in ^{48}Ca. This interaction provides only the 2^+ state at 2.8MeV. Here, the neutron number is magic and the 2^+ level is from one neutron excited across the $N = 28$ shell. The datum 3.8MeV in level 2^+ of ^{48}Ca marks an energy gap of $N = 28$ and determines the strength of the monopole terms $Mc3$ and $Mc4$. With their monopole effects, the calculations reproduced the data for the 2^+ and 4^+ states very well (Fig. 5a,b). As

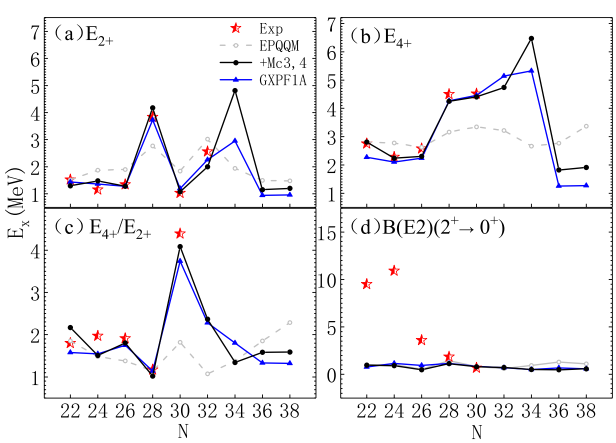

Fig. 5 Experimental 2^+, 4^+ states, $B(E2)$ values from 2^+ to 0^+ [41], and the shell model calculations by EPQQM and a set of effective interactions. Label $+Mc3,4$ means including the monopole effects of $Mc3$ and $Mc4$

indicated by the black solid points, we predict the 2^+ state of ^{54}Ca at approximately 5 MeV. This implies that the energy gap for $N = 34$ is higher than that for the magic number $N = 28$. which supports “a new nuclear magic number from the level structure of ^{54}Ca" [1].

As shown in Fig. 5, the EPQQM with the monopole effects of Mc3 and Mc4 reproduced the level structure of the Ca isotopes from $N = 22$ to $N = 30$. For configurations, the 2^+ state of ^{48}Ca has 77.46% of $\nu f^7_{7/2}p_{3/2}$, and 6.98% of $\nu f^6_{7/2}p^2_{3/2}$. This state is almost entirely composed of one neutron excited across the $N = 28$ shell. The 2^+ state of ^{46}Ca is 85% of $\nu f^6_{7/2}$ and 4.38% of $\nu f^5_{7/2}p_{3/2}$ and the component crossing $N = 28$ is very small. In ^{54}Ca, the 2^+ state is 89.96 % of $\nu f_{5/2}p_{1/2}$. Orbits $\nu f_{7/2}$ and $\nu p_{3/2}$ are completely occupied. The high energy of the 2^+ state indicates an energy gap between orbits $\nu f_{5/2}$ and $\nu p_{1/2}$.

In the Ca isotopes from $N = 22$ to $N = 38$, the monopole effects of $Mc3$ and $Mc4$ have almost no impact on the $B(E2)$ values from the 2^+ to 0^+ states. Both the set of effective interactions and the interactions in Ref. [36] yielded $B(E2)$ values near zero (Fig. 5d). The experimental data exhibited a peak at ^{44}Ca, followed by a general decrease in the $B(E2)$ values for isotopes with higher neutron numbers (beyond ^{44}Ca). Theoretical models generally predict lower and more stable $B(E2)$ values near zero. The $Mc3,4$ monopole effects partially capture the overall trend observed in the experimental data, although they underestimate the values for ^{44}Ca and ^{46}Ca. This discrepancy suggests potential limitations in the ability of the model to fully capture the specific nuclear structure effects that influence $B(E2)$ transitions in this isotopic chain.

4 Summary

The level spectra and monopole effects of the Ca isotopes were investigated using a model space that included the pf shell and the intruder orbital $g_{9/2}$. This study enhances the understanding of the energy spectrum by considering the effects of the intruder orbit $g_{9/2}$. The EPQQM with the monopole effects of $Mc3$ and $Mc4$ reproduced the level structure of Ca isotopes from $N = 22$ to $N = 30$, and the main conclusions are as follows:

(1) In ^{44}Ca, positive-parity states are effectively reproduced. The negative-parity states coupled with the intruder orbital $g_{9/2}$ are predicted to be approximately 4 MeV.
(2) In $^{46-58}$Ca, we reproduced the existing data well; for example, 1^+, 3^+, and 5^+ in ^{46}Ca, and 5^+, 6^+ in ^{48}Ca. The excited states 2^+ and 4^+ in ^{50}Ca were close to the

experimental data, whereas the 2^+ and 4^+ states provided good predictions for ^{54}Ca.

(3) For the Ca isotopes from $N = 22$ to $N = 38$, both E_{2+} and E_{4+} reached peak values at the neutron magic number $N = 28$. The values of E_{4^+}/E_{2^+} reproduce the experimental trend from ^{42}Ca to ^{50}Ca.

(4) With the monopole effects between $\nu f_{7/2}$ and $\nu p_{3/2}$ ($\nu f_{5/2}$) in data of ^{48}Ca and ^{50}Ca, the EPQQM interaction predicts a high-energy 2^+ state in ^{54}Ca, which supports a new nuclear magic number from the level structure of ^{54}Ca.

Author contributions All authors contributed to the study conception and design. Material preparation, data collection and analysis were performed by Jin Li, Ai-Xi Chen, Amir Jalili, and Han-Kui Wang. The first draft of the manuscript was written by Jin Li and all authors commented on previous versions of the manuscript. All authors read and approved the final manuscript.

Data availability The data that support the findings of this study are openly available in Science Data Bank at https://cstr.cn/31253.11.sciencedb.j00186.00240 and https://doi.org/10.57760/sciencedb.j00186.00240.

Declarations

Conflict of interest The authors declare that they have no conflict of interest.

References

1. D. Steppenbeck, S. Takeuchi, N. Aoi et al., Evidence for a new nuclear 'magic number' from the level structure of ^{54}Ca. Nature **502**, 207–210 (2013). https://doi.org/10.1038/nature12522
2. O. Sorlina, M.-G. Porquet, Nuclear magic numbers: new features far from stability. Prog. Part. Nucl. Phys. **61**, 602–673 (2008). https://doi.org/10.1016/j.ppnp.2008.05.001
3. T. Otsuka, Exotic nuclei and nuclear forces. Phys. Scr. **152**, 014007 (2013). https://doi.org/10.1088/0031-8949/2013/T152/014007
4. C. Détraz, D. Guillemaud, G. Huber et al., Beta decay of $^{27\text{-}32}$Na and their descendants. Phys. Rev. C **19**, 164 (1979). https://doi.org/10.1103/PhysRevC.19.164
5. D. Guillemaud-Mueller, C. Detraz, M. Langevin et al., β-Decay schemes of very neutron-rich sodium isotopes and their descendants. Nucl. Phys. A **426**, 37–76 (1984). https://doi.org/10.1016/0375-9474(84)90064-2
6. T. Motobayashi, Y. Ikeda, K. Ieki et al., Large deformation of the very neutron-rich nucleus ^{32}Mg from intermediate-energy Coulomb excitation. Phys. Lett. B **346**, 9–14 (1995)
7. B. Bastin, S. Grévy, D. Sohler et al., Collapse of the $N = 28$ shell closure in ^{42}Si. Phys. Rev. Lett. **99**, 022503 (2007). https://doi.org/10.1103/PhysRevLett.99.022503
8. S. Takeuchi, M. Matsushita, N. Aoi et al., Well developed deformation in ^{42}Si. Phys. Rev. Lett. **109**, 182501 (2012). https://doi.org/10.1103/PhysRevLett.109.182501
9. C.R. Hoffman, T. Baumann, D. Bazin et al., Determination of the $N = 16$ shell closure at the oxygen drip line. Phys. Rev. Lett. **100**, 152502 (2008). https://doi.org/10.1103/PhysRevLett.100.152502
10. C.R. Hoffman, T. Baumann, D. Bazin et al., Evidence for a doubly magic ^{24}O. Phys. Lett. B **672**, 17–21 (2009). https://doi.org/10.1016/j.physletb.2008.12.066
11. R. Kanungo, C. Nociforo, A. Prochazka et al., One-neutron removal measurement reveals ^{24}O as a new doubly magic nucleus. Phys. Rev. Lett. **102**, 152501 (2009). https://doi.org/10.1103/PhysRevLett.102.152501
12. F. Wienholtz, D. Beck, K. Blaum et al., Masses of exotic calcium isotopes pin down nuclear forces. Nature **498**, 346–349 (2013). https://doi.org/10.1038/nature12226
13. S. Chen, J. Lee, P. Doornenbal et al., Quasifree neutron Knockout from ^{54}Ca corroborates arising $N = 34$ neutron magic number. Phys. Rev. Lett. **123**, 142501 (2019). https://doi.org/10.1103/PhysRevLett.123.142501
14. M. Tanaka, M. Takechi, A. Homma et al., Swelling of doubly magic ^{48}Ca core in Ca isotopes beyond $N = 28$. Phys. Rev. Lett. **124**, 102501 (2020). https://doi.org/10.1103/PhysRevLett.124.102501
15. L. Zhou, S.M. Wang, D.Q. Fang et al., Recent progress in two-proton radioactivity. Nucl. Sci. Tech. **33**, 105 (2022). https://doi.org/10.1007/s41365-022-01091-1
16. X. Zhou, M. Wang, Y.H. Zhang et al., Charge resolution in the isochronous mass spectrometry and the mass of ^{51}Co. Nucl. Sci. Tech. **32**, 37 (2021). https://doi.org/10.1007/s41365-021-00876-0
17. X.B. Wei, H.L. Wei, Y.T. Wang et al., Multiple-models predictions for drip line nuclides in projectile fragmentation of ^{40,48}Ca, ^{58,64}Ni, and ^{78,86}Kr at 140 MeV/u. Nucl. Sci. Tech. **33**, 155 (2022). https://doi.org/10.1007/s41365-022-01137-4
18. E.B. Huo, K.R. Li, X.Y. Qu et al., Continuum Skyrme Hartree–Fock–Bogoliubov theory with Green's function method for neutron-rich Ca, Ni, Zr, and Sn isotopes. Nucl. Sci. Tech. **34**, 105 (2023). https://doi.org/10.1007/s41365-023-01261-9
19. P.H. Chen, H. Wu, Z.X. Yang et al., Prediction of synthesis cross sections of new moscovium isotopes in fusion-evaporation reactions. Nucl. Sci. Tech. **34**, 7 (2023). https://doi.org/10.1007/s41365-022-01157-0
20. Y.F. Gao, B.S. Cai, C.X. Yuan et al., Investigation of β^- decay half-life and delayed neutron emission with uncertainty analysis. Nucl. Sci. Tech. **34**, 9 (2023). https://doi.org/10.1007/s41365-022-01153-4
21. Y.Z. Ma, L. Coraggio, L. De Angelis et al., Contribution of chiral three-body forces to the monopole component of the effective shell-model Hamiltonian. Phys. Rev. C **100**, 034324 (2019). https://doi.org/10.1103/PhysRevC.68.044317
22. A.A. Raduta, L. Zamick, E. Moya de Guerra et al., Description of single and double analog states in the $f_{7/2}$ shell: the Ti isotopes. Phys. Rev. C **68**, 044317 (2003). https://doi.org/10.1103/PhysRevC.68.044317
23. A. Juodagalvis, I. Ragnarsson, S. Aberg, Cranked Nilsson-Strutinsky vs the spherical shell model: a comparative study of pf-shell nuclei. Phys. Rev. C **73**, 044327 (2006). https://doi.org/10.1103/PhysRevC.73.044327
24. M. Honma, T. Otsuka, B.A. Brown et al., Shell-model description of neutron-rich pf-shell nuclei with a new effective interaction GXPF1. Eur. Phys. J. A **25**, 499 (2005). https://doi.org/10.1140/epjad/i2005-06-032-2
25. M. Hasegawa, K. Kaneko, Extension of the pairing plus quadrupole force model to $N \approx Z$ nuclei. Phys. Rev. C **59**, 1449 (1999). https://doi.org/10.1103/PhysRevC.59.1449
26. M. Hasegawa, K. Kaneko, S. Tazaki, Improvement of the extended P + QQ interaction by modifying the monopole field. Nucl. Phys. A **688**, 765 (2001). https://doi.org/10.1016/S0375-9474(00)00602-3

27. K. Kaneko, M. Hasegawa, T. Mizusaki, Quadrupole and octupole softness in the $N = Z$ nucleus ^{64}Ge. Phys. Rev. C **66**, 051306(R) (2002). https://doi.org/10.1103/PhysRevC.66.051306
28. K. Kaneko, Y. Sun, M. Hasegawa et al., Shell model study of single-particle and collective structure in neutron-rich Cr isotopes. Phys. Rev. C **78**, 064312 (2008). https://doi.org/10.1103/PhysRevC.78.064312
29. K. Kaneko, Y. Sun, T. Mizusaki et al., Shell-model study for neutron-rich *sd*-shell nuclei. Phys. Rev. C **83**, 014320 (2011). https://doi.org/10.1103/PhysRevC.83.014320
30. H.K. Wang, S.K. Ghorui, Z.Q. Chen et al., Analysis of low-lying states, neutron-core excitations, and electromagnetic transitions in tellurium isotopes $^{130\text{-}134}$Te. Phys. Rev. C **102**, 054316 (2020). https://doi.org/10.1103/PhysRevC.102.054316
31. H.K. Wang, S.K. Ghorui, K. Kaneko et al., Large-scale shell-model study for excitations across the neutron $N = 82$ shell gap in $^{131\text{-}133}$Sb. Phys. Rev. C **96**, 054313 (2017). https://doi.org/10.1103/PhysRevC.96.054313
32. H.K. Wang, Y. Sun, H. Jin et al., Structure analysis for hole-nuclei close to ^{132}Sn by a large-scale shell-model calculation. Phys. Rev. C **88**, 054310 (2013). https://doi.org/10.1103/PhysRevC.88.054310
33. H.K. Wang, K. Kaneko, Y. Sun, Isomerism and persistence of the $N = 82$ shell closure in the neutron-rich ^{132}Sn region. Phys. Rev. C **89**, 064311 (2014). https://doi.org/10.1103/PhysRevC.89.064311
34. H.K. Wang, K. Kaneko, Y. Sun et al., Monopole effects, isomeric states, and cross-shell excitations in the $A = 129$ hole nuclei near ^{132}Sn Phys. Rev. C **95**, 011304 (2017). https://doi.org/10.1103/PhysRevC.95.011304
35. H.K. Wang, H. Yang, M.L. Liu et al., Ground-state inversion: the monopole-force governance in neutron mid-shell region. Phys. Lett. B **849**, 138449 (2024). https://doi.org/10.1016/j.physletb.2024.138449
36. J.Z. Han, S. Xu, H.K. Wang et al., Investigation of the level spectra of nuclei in the northeast region of doubly magic ^{40}Ca with intruder orbit $g_{9/2}$. Nucl. Sci. Tech. **34**, 85 (2023). https://doi.org/10.1007/s41365-023-01243-x
37. H.K. Wang, Y.J. Li, Y.B. Wang et al., Spectroscopic factors and level spectra in neutron-rich Sn isotopes. Phys. Rev. C **107**, 064305 (2023). https://doi.org/10.1103/PhysRevC.107.064305
38. A.J. Majarshin, Y.A. Luo, F. Pan et al., Nuclear structure and band mixing in ^{194}Pt. Phys. Rev. C **103**, 024317 (2021). https://doi.org/10.1103/PhysRevC.103.024317
39. A.J. Majarshin, Y.A. Luo, F. Pan et al., Structure of rotational bands in ^{109}Rh. Phys. Rev. C **104**, 014321 (2021). https://doi.org/10.1103/PhysRevC.104.014321
40. B.A. Brown, W.D.M. Rae, The shell-model code NuShellX@MSU. Nucl. Data Sheets **120**, 115 (2014). https://doi.org/10.1016/j.nds.2014.07.022
41. http://www.nndc.bnl.gov/ensdf/